

doi: 10.2306/scienceasia1513-1874.2025.068

MicroRNA-146a-5p alleviates bronchopulmonary dysplasia in neonatal mice by modulating the TGF-β1/SMAD4 pathway

Shuning Zhang^a, Luyao Lin^a, Yueling Li^a, Liyu Liang^{a,b}, Qinmei Xie^{a,b}, Yongle Liu^{a,b}, Yan Lin^{a,b}, Jiyu Huang^{a,b}, Meijun Yang^{a,b}, Xiaohui Chen^{b,c}, Fuli Wen^{b,d}, Xiaochun Zheng^{b,c,*}, Hui Zhu^{a,b,e,*}

- ^a Department of NICU, Shengli Clinical Medical College of Fujian Medical University, Fuzhou 350001 China
- b Department of Children's Health Prevention of Fuzhou University Affiliated Provincial Hospital, Fuzhou 350001 China
- ^c Department of Anesthesiology, Shengli Clinical Medical College of Fujian Medical University, Fuzhou 350001 China
- d Center for Experimental Research in Clinical Medicine, Fujian Provincial Hospital, Shengli Clinical Medical College of Fujian Medical University, Fuzhou 350001 China
- ^e Fujian Provincial Key Laboratory of Critical Care Medicine, Fuzhou 350001 China

Received 6 May 2025, Accepted 11 Jul 2025 Available online 30 Aug 2025

ABSTRACT: Bronchopulmonary dysplasia (BPD) is a common and challenging disease that affects newborns and infants, characterized by alveolar dysplasia and reduced pulmonary function. Various microRNAs (miRNAs) have been found to be deferentially expressed during the progression of BPD. The interaction between SMAD4 and miR-146a-5p was identified using a dual-luciferase reporter assay. A mouse model of BPD was established through hyperoxia induction, where the expression pattern of miR-146a-5p, pathological manifestations, and fibrosis factors were assessed over 14 days. Additionally, lentivirus-packed vectors were used to modulate miR-146a-5p expression in mice to observe its effects. SRI-011381 was employed to activate TGF- β 1, confirming that miR-146a-5p targets SMAD4 and influences the TGF- β pathway in BPD progression. The expressions of miR-146a-5p, TGF- β 1, and SMAD4 in BPD neonatal mice were determined using RT-qPCR and Western blot analysis, while TGF- β 1, COL I, and COL III levels were evaluated through immunohistochemistry semi-quantification. We found miR-146a-5p was up-regulated in the lung tissues of hyperoxia-induced BPD neonatal mice over time. SMAD4 was identified as a target of miR-146a-5p which was shown to down-regulate SMAD4, thereby inactivating the TGF- β signaling pathway. This resulted in decreased expression of fibrosis factors and restoration of alveolarization in BPD neonatal mice. Our findings demonstrate that miR-146a-5p facilitates alveolarization in preterm neonates with BPD by suppressing the SMAD4-dependent TGF- β pathway.

KEYWORDS: bronchopulmonary dysplasia, neonate, respiratory, TGF-β/SMAD4 signal pathway, microRNA

INTRODUCTION

Bronchopulmonary dysplasia (BPD) is the most common chronic respiratory disease in premature infants [1]. The immature lung is affected by genetic factors and various environmental influences, leading to injury and abnormal repair processes [2]. The main characteristics of BPD are alveolar and pulmonary vascular dysplasia, with clinical manifestations including long-term oxygen dependence and progressive dyspnea. Clinical diagnosis and treatment of BPD are often delayed, and early biological markers are lacking [3]. Numerous studies have shown that various growth factors, proteins, and related signaling pathways exhibit expression disorders in the early stages of BPD development [4-7]. In-depth research and elucidation of these signaling pathways are crucial for the prevention and early treatment of BPD.

MicroRNA (miRNA) is a single-stranded, small RNA molecule approximately 21 to 23 bases in length [8]. miRNA constitutes a highly conserved class of genes, indicating a significant biological function. Research has demonstrated that miRNAs are involved in a variety of physiological and pathological

processes, including the regulation of developmental processes, resistance to viral invasion, modulation of animal immune function, and various diseases affecting organs or systems, as well as in different stages of tumorigenesis [9]. miRNAs can modulate gene expression at the post-transcription level by binding to the 3' untranslated region (3'UTR) of gene transcripts, thereby inhibiting their translation or inducing their degradation. They typically regulate multiple target genes within the same biological pathway.

Among these miRNAs, miR-146a-5p has been extensively studied and found to be closely associated with molecular pathways involving fibrosis and inflammation [10–13]. Particularly in diseases such as liver fibrosis, cystic fibrosis, and obliterative bronchiolitis, the levels of miR-146a-5p are closely associated with the progression of the disease [14–16]. Despite its extensive study, the expression levels and roles of miR-146a-5p in BPD models, which are also characterized by alveolar fibrosis, remain unclear and merit further investigation and exploration.

The Transforming Growth Factor Beta (TGF- β) signaling pathway is implicated in various cellular processes during organismal and embryonic development,

^{*}Corresponding authors, e-mail: zhengxiaochun@fisl.com.cn, zhuhui6154@163.com

including fibrosis [17,18]. SMAD4, a key mediator receptor downstream of TGF- β 1, plays a critical role in transmitting TGF- β 1 signals from the cytoplasm to the nucleus [19]. Collagen I (COL I) and Collagen III (COL III) are major components of collagen fibers in tissue fibrosis, with their levels significantly increasing in lung tissue during pulmonary fibrosis.

Therefore, this study investigates the role of miR-146a-5p in the progression of BPD, discusses its specific mechanisms in BPD-related pulmonary fibrosis and its connection with SMAD4, with the aim of providing preclinical evidence for the diagnosis and treatment of BPD.

MATERIALS AND METHODS

Bioinformatic analysis

Using TargetScan 7.2 (http://www.targetscan.org/ miRDB (http://www.Mirdb.org/) and vert 72), miRWalk 3.0 (http://www.umm.uni-heidel-berg. de/apps/zmf/mirwalk/) to predict target genes hsa-miR-146a-5p, Venn diagram a constructed using the R package Venn to depict the intersection of these databases. Subsequently, validated target genes of hsa-miR-146a-5p with strong experimental evidence were obtained from miRTarBase (http://mirtarbase.mbc.Nctu.edu.tw) and merged with the intersection of the aforementioned target genes to form a new gene set. Utilizing RStudio software and the R package clusterProfiler, differential gene expression data underwent Gene Ontology (GO) functional annotation analysis. GO annotation consists of three categories: molecular function, cellular component, and biological process, with GO terms corrected for p < 0.05 considered significantly enriched.

Dual luciferase reporter gene assay

Based on the PCR-based Accurate Synthesis (PAS) method, full-length overlapping primers were designed to synthesize SMAD4 (NM_005359.6) wild-type (WT) and mutant (MUT) sequences through two rounds of PCR. These sequences were then separately ligated into the psicheck2.0 vector to obtain recombinant SMAD4 WT and SMAD4 MUT vectors. Additionally, hsa-miR-146a-5p mimics were synthesized *in vitro*. Transfection into 293T cells was performed using Lipofectamine 3000, and the regulatory effect of hsa-miR-146a-5p mimics on the SMAD4 gene was assessed using dual-luciferase reporter assays. The materials for this study were purchased from Zaiji Biotechnology Co., Ltd., Fuzhou, China.

Establishment of hyperoxia induced BPD neonatal mice models and grouping

SD mice were purchased from Sipeifu Biotech Company (Beijing, China). All animal experiments were

conducted in strict accordance with protocols approved by the Ethics Committee of the Fujian Provincial Hospital (IACUC-FPH-SL-20230625[0005]). custom-made oxygen chamber (sealed plastic storage box, dimensions 60 cm × 35 cm × 30 cm) was used for oxygen exposure, equipped with air inlets, outlets, and oxygen monitoring ports. Soda lime was used to absorb CO2, and anhydrous silica gel was used to absorb moisture. The chamber's temperature was maintained between 22 °C and 27 °C, and humidity was kept between 50% and 70%. Mice in the air control group were housed in a standard breeding cage under identical conditions to the hyperoxia group, except that they breathed room air instead of oxygen. Every day at 9:00 AM, the chamber was opened for 1 h to provide fresh water and food and to replace the bedding. To prevent feeding impairment caused by oxygen toxicity, mother mice in the oxygen and air groups were exchanged daily. The weight and condition of the newborn mice were monitored daily. The oxygen concentration in the hyperoxia group was maintained at 60%, while the control group was kept at 21%. These conditions were maintained throughout the experiment.

The hyperoxia-treated mice were classified into the miR-146a-5p negative control named as BPD+shNC group (BPD mice inhale with lentiviral empty vector), BPD+miR group (BPD mice infected with lentiviral particles expressing miR-146a-5p agomir), BPD+SRI group (BPD mice infected with TGF-β1 agonist), BPD+DMSO (BPD mice infected with TGF-β1 agonist dissolvent), BPD+miR+SRI group (BPD mice infected with lentiviral particles expressing miR-146a-5p agomir and TGF-β1 agonist) and BPD group (n = 5 for each treatment). The neonatal mice were raised to D4 and then inhaled with 5 µl lentiviral vector expressing miR-146a-5p agomir (2.0×10^9) TU/ml) or none. This procedure was conducted only on D4 for once. The SRI-011381 (Selleck, Houston, USA) or the DMSO as the TGF-β1 agonist and dissolvent were also given by intraperitoneal injection every two days from D4 until the end of the experiment. The air group was also raised for 14 days as negative control (NC) group for comparing.

On the D4, 7 and 14, the groups of mice were received an intraperitoneal injection of 100 mg/kg phenobarbital sodium for euthanasia. The euthanasia of mice for intervention studies were conducted only on the 14th day. Next, the abdominal cavity was immediately opened, and the right lung was removed and placed in an RNase-free cryovial (Eppendorf, Hamburg, Germany). After rapid freezing with liquid nitrogen, the lungs were stored in a -80 °C refrigerator for subsequent reverse transcription quantitative polymerase chain reaction (RT-qPCR) and Western blot analysis. Next, 40 g/l paraformaldehyde was slowly injected into the mice through the left bronchus until the apex of the lung was inflated. The lung was placed

in an embedding box, and 40 g/l paraformaldehyde solution was added for overnight fixation and subsequent use.

Histological analysis

Lung tissues of mice in each group were collected on the 14th day of modeling, fixed with 4% paraformaldehyde for 24 h, sequentially dehydrated with 100%, 90%, 80%, 70%, 50% ethanol respectively, and immersed in a wax box at 60 °C. Following xylene dewaxing and hydration, the sections were first stained with hematoxylin (Servicebio, Wuhan, China) for 2 min and then with eosin for 1 min, followed by gradient ethanol dehydration, xylene clearing, and neutral rubber fixing. Finally, the morphological changes in lung tissues were observed and analyzed under an optical microscope. Radial alveolar counts (RAC) and mean linear intercept (MLI) were counted to estimate the quantity and size of the alveolus using the Image pro Plus 6. For each group, five mice were selected, and sections were examined under a light microscope at 100× magnification. Five random fields of view were chosen for counting the RAC and MLI.

Immunohistochemistry

Lung's paraffin slices were dewaxed and hydrated. Then pretreated, and incubated with primary antibody COL1A (PB9939, 1:400, Boster, Pleasanton, USA) and COL3A1 (A0078-3, 1:2000, Boster) followed by goat anti-rabbit IgG H&L. These slices were observed and photographed under an optical microscope. Ten fields were randomly selected from five sections after 200× magnification, and the cytoplasm was counted as positive cells. The ImagePro Plus image analysis software was applied to determine the IOD (integral optical density) of all positive cells after removing the background optical density value and divided by the corresponding positive cell area to obtain the average integrated optical density AOD (average optical density).

Western blot analysis

The lung tissues were added to lysis buffer, shaken on a vortex agitator, and centrifuged at 12000× g for 30 min at 4°C to remove tissues debris. Using RIPA lysis buffer containing PMSF, total protein was isolated from cells. Protein concentration was determined using the BCA Protein Assay Kit PC 0020-500. SDS-PAGE (10%) was performed to separate the proteins based on previous studies. After separation, the bands were transferred onto nitrocellulose membranes, which were then blocked with 5% bovine serum albumin at room temperature for 2 h. After blocking, the PVDF membranes were incubated overnight at 4°C with antibodies against β-actin (1:1000, ab8226, Abcam, Cambridge, UK), SMAD4 (1:500, 10231-1-AP, Proteintech, Wuhan, China), and TGF-β1 (1:1000, 21898-1-AP, Proteintech), respectively. The membranes were then washed with TBS and incubated with a secondary antibody diluted 1:5000 at room temperature for 2 h. Subsequently, signals were collected using the Thermo ECL chemiluminescence system (34080; Thermo Fisher Scientific, Inc., Waltham, USA). The results were analyzed using the Versa Doc imaging system (Shanghai Bioequi Technology Co., Ltd., China) and ImageJ software (V1.8.0.112, National Institutes of Health). Ratio of the grey value of the target band to β -actin was considered representative of the relative protein expression. The experiment was conducted three times for each group of mice, with the mean values being calculated from the results.

RT qPCR

The tissue specimens of 5 mice from each group were ground into a powder with liquid nitrogen and further transferred to a 1.5 ml eppendorf tube. Total RNA was extracted from cells using NucleoZol (Thermo Fisher Scientific Inc.). A total of 5 μg RNA was reversely transcribed into cDNA in accordance to the instructions of RT-qPCR (Applied Biosystems Inc., CA, USA). The primer sequences are displayed in Table S1. U6 was used as an internal reference of miR-146a-5p and the β -actin was used as an internal reference of SMAD4. The ratio of the expression of the target gene between the experimental and control groups was calculated using the $2^{-\Delta\Delta Ct}$ method and performed with triplicate technical replicates for each sample.

Statistical analysis

Utilizing SPSS 27.0 software for statistical analysis, statistical graphs were generated using GraphPad Prism 7 software, while schematic diagrams were created using BioRender and Photoshop. Measurement data were summarized as mean \pm standard deviation. Data comparisons between multiple groups were performed using one-way analysis of variance (ANOVA), followed by a Tukey's multiple comparisons post hoc test. Data comparisons at different time points were performed by two-way ANOVA, followed by a Bonferroni post hoc test for multiple comparisons. Statistical significance was defined as p < 0.05.

RESULTS

miR 146a-5p is predicted to orchestrate SMAD4 expression and mediate the TGF- $\beta 1$ pathway in BPD

The predicted downstream target genes of miR-146a-5p were identified using the TargetScan, miRWalk, and miRDB databases, and the results were visualized using a Venn diagram (Fig. 1A). A dataset containing 28 target genes was obtained. Additionally, 29 target genes with strong experimental evidence were sourced from miRTarBase. After merging these datasets, a total of 57 candidate genes were identified, forming a set of target genes (hsa-miR-146a-5p). This target

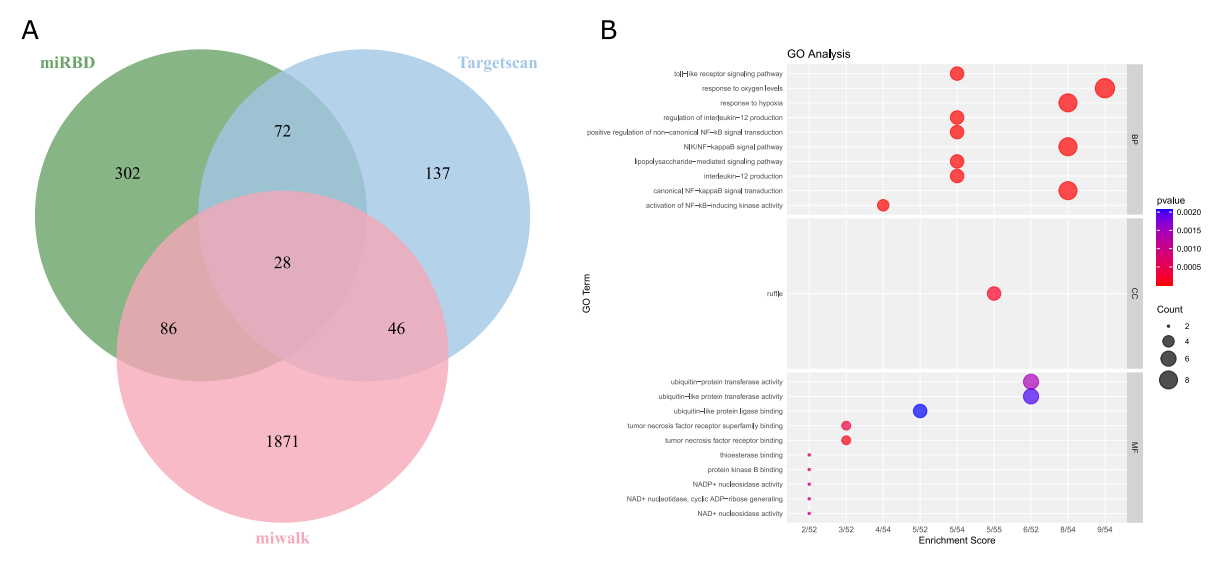


Fig. 1 The miR-146a-5p/TGF β 1/SMAD4 axis is predicted to be involved in BPD. (A) The Venn diagram depicting the intersection of target mRNAs of miR-146a-5p predicted by the TargetScan, miRWalk and miRDB databases. (B) GO analysis of the target gene of miR-146a-5p show top 10 terms of biological process and 1 cellular component, 10 molecular function.



Fig. 2 mmu-miR-146a-5p targets SMAD4. (A) mircoRNA.org website predicates that mmu-miR-146a-5p binds to the 3'-UTR of SMAD4. (B) The luciferase activity is detected after treatment by a combination of mmu-miR-146a-5p and SMAD4-3'UTR-WT by dual luciferase reporter gene assay.

gene set underwent GO functional enrichment analysis, which revealed statistically significant enrichment in 251 biological processes (with the top 10 most significantly enriched processes selected for analysis), one molecular function, and 10 cellular components (Fig. 1B). Among these, the biological process related to the response to oxygen concentration was particularly noteworthy. This process includes the target gene SMAD4, a common mediator of the TGF-β signaling pathway. In this pathway, SMAD4 forms complexes with SMAD2/3, which are activated upstream, and participates in transcriptional regulation. Several studies have demonstrated the close association between the upregulation of the TGF-β1 signaling pathway and bronchopulmonary dysplasia. Based on these data, we hypothesized that miR-146a-5p could regulate the expression of SMAD4 and thereby modulate the TGF-

 $\beta 1$ pathway, influencing the progression of BPD in preterm infants.

The search for target prediction database shows that mmu-miR-146a-5p and the wild-type (WT) 3'UTR of SMAD4 have corresponding binding sites (Fig. 2A). In this study, plasmids containing WT- and MUT-SMAD4 were constructed and transfected into 293T cells along with miR-146a-5p mimics or NC mimics. Luciferase activity was then measured (Fig. 2B). The results showed that the luciferase activity of the miR-146a-5p mimics+SMAD4 3'UTR WT group was significantly reduced compared to the NC mimics+SMAD4 3'UTR WT group (p < 0.05). There was no significant change in luciferase activity between the miR-146a-5p mimics+SMAD4 3'UTR MUT group (p > 0.05). Thus, miR-146a-5p significantly reduces the luciferase activ

ity of the SMAD4-WT group, but does not affect the luciferase activity of the SMAD4-MUT group. These results indicate that miR-146a-5p can target and bind to SMAD4. Based on these data, we hypothesized that miR-146a-5p could regulate the expression of SMAD4 and further regulate the TGF-β1 pathway, thus affecting the progression of BPD in neonatal mice.

miR 146a-5p is upregulated in the lung tissues of hyperoxia induced BPD neonatal mice

To verify the above hypothesis, a hyperoxia-induced neonatal mice model with BPD was established. In the NC group, the mice exhibited overall good health postnatally. Conversely, in the BPD group, prolonged exposure to high oxygen levels led to a progressive decline in activity and responsiveness. The mice developed mild cyanosis in toes, the fur became sparse and dull, respiration rate increased, and weight gain was slow (Fig. 3A). RT-qPCR data showed that the expression of miR-146a-5p in the BPD group increased in a time dependent manner (Fig. 3B). Only on the 14th day, it was significant higher in neonatal mice with BPD than in the NC group. H&E staining was used to observe lung tissue morphology in BPD mice. The lung tissue structure of the air and hyperoxia groups was observed under low power lens. In the BPD group, as the age of mice increased, microscopic observation of lung tissue development revealed fused lung tissue patches, widening of some alveolar septa, vascular dilation with congestion in alveolar septa, increased fibrous tissue proliferation around bronchi, and focal accumulation of inflammatory cells (Fig. 3C). The RAC and MLI value compared to the NC group showed that with exposure to hyperoxia prolonged (Fig. 3D), the number of the alveoli and alveolar diameter increased significantly in the hyperoxia group (p < 0.05). Overall, lung tissue in the BPD group exhibited signs of inhibited lung development under microscopic examination. Compared with NC group, BPD neonatal mice exhibited persistent high levels of fibrosis factors (COL I, COL III) (Fig. 3E,F).

Overexpression of miR-146a-5p restored alveolarization and reduced fibrosis in neonatal mice with BPD

We further investigated the effects of miR-146a-5p on hyperoxia-induced BPD in neonatal mice. After inhalation of miR-146a-5p agomir, miR-146a-5p expression was significantly elevated in the lung tissue of BPD mice, while the BPD+shNC ones showed no changes with the lentivirus vector inhalation (Fig. 4A). Compared to the BPD group, the BPD+miR group showed only slight hemorrhage in H&E staining, and the parabronchial fibrous tissue exhibited only minimal hyperplasia (Fig. 4B). These trends, indicated by the values of RAC and MLI, also demonstrated a reduction in the number of alveoli and a decrease in alveolar

diameter (Fig. 4C). These results indicate that overexpression of miR-146a-5p can promote alveolarization in neonatal mice with BPD. Additionally, the increased levels of collagen in the lungs were reversed by miR-146a-5p agomir treatment, as shown by immunohistochemistry (Fig. 4D,E), suggesting its effect on reducing fibrosis.

Taken together, our results confirmed that overexpression of miR-146a-5p restored alveolarization and reduced fibrosis in the BPD mice.

miR-146a-5p could target SMAD4 to alleviate the alveolar damage induced by TGF- $\beta1$ pathway activation

To elucidate the regulatory mechanism of miR-146a-5p through the TGF-β1 pathway in influencing BPD progression, neonatal mice with BPD were then treated with SRI-011381 to activate TGF-β1, and DMSO to exclude the effect of the solvent. The lung tissue pathology and morphology in the BPD+DMSO group mice were similar to those in the BPD group mice. While compared to the BPD group, the BPD+SRI one was poor, with increased inflammation exudation, thicker alveolar septa, more pronounced alveolar cavity enlargement, significantly increased average intercept, and markedly reduced radial alveolar counts. The above trends could be reversed by the administration of miRNA-146a-5p agomir in the BPD+SRI+miR group, with significantly decreased of MLI value, and markedly increased RAC value. Overall pathological findings were better observed compared to the BPD+SRI group (Fig. 5A,B).

Using RT-qPCR analysis, we investigated the interaction between miR-146a-5p and SMAD4. In comparison with the BPD group, the level of SMAD4 mRNA expression in the BPD+miR group decreased significantly, while the level of miR-146a-5p increased significantly. The same trend when comparing the BPD+SRI to the BPD+SRI+miR group, with the level of miR-146a-5p increased significantly and the SMAD4 decreased (p < 0.05) (Fig. 5C,D). Western blot analysis showed that SMAD4 expression was increased in the lung tissue of neonatal mice exposed to hyperoxia, and was further enhanced in the BPD+SRI group. Increasing the level of miR-146-5p could decrease the level of SMAD4 expression in the BPD+SRI+miR group. However, the expression level of TGF-β1 was not affected by the presence of miR-146a-5p, it was significantly increased only after SRI-011381 treatment, as shown in Western blot and immunohistochemistry analysis (Fig. 5E,H). Downstream factors like COL I, and COL III, were most significantly expressed in the BPD+SRI group (p < 0.05). Following this, based on the significant expression levels, the order from highest to lowest was the BPD+miR+SRI group, the BPD group, and the BPD+miR group (p < 0.05) (Fig. 5F,G).

These results indicated that overexpression of miR-146a-5p could target SMAD4 to regulate the

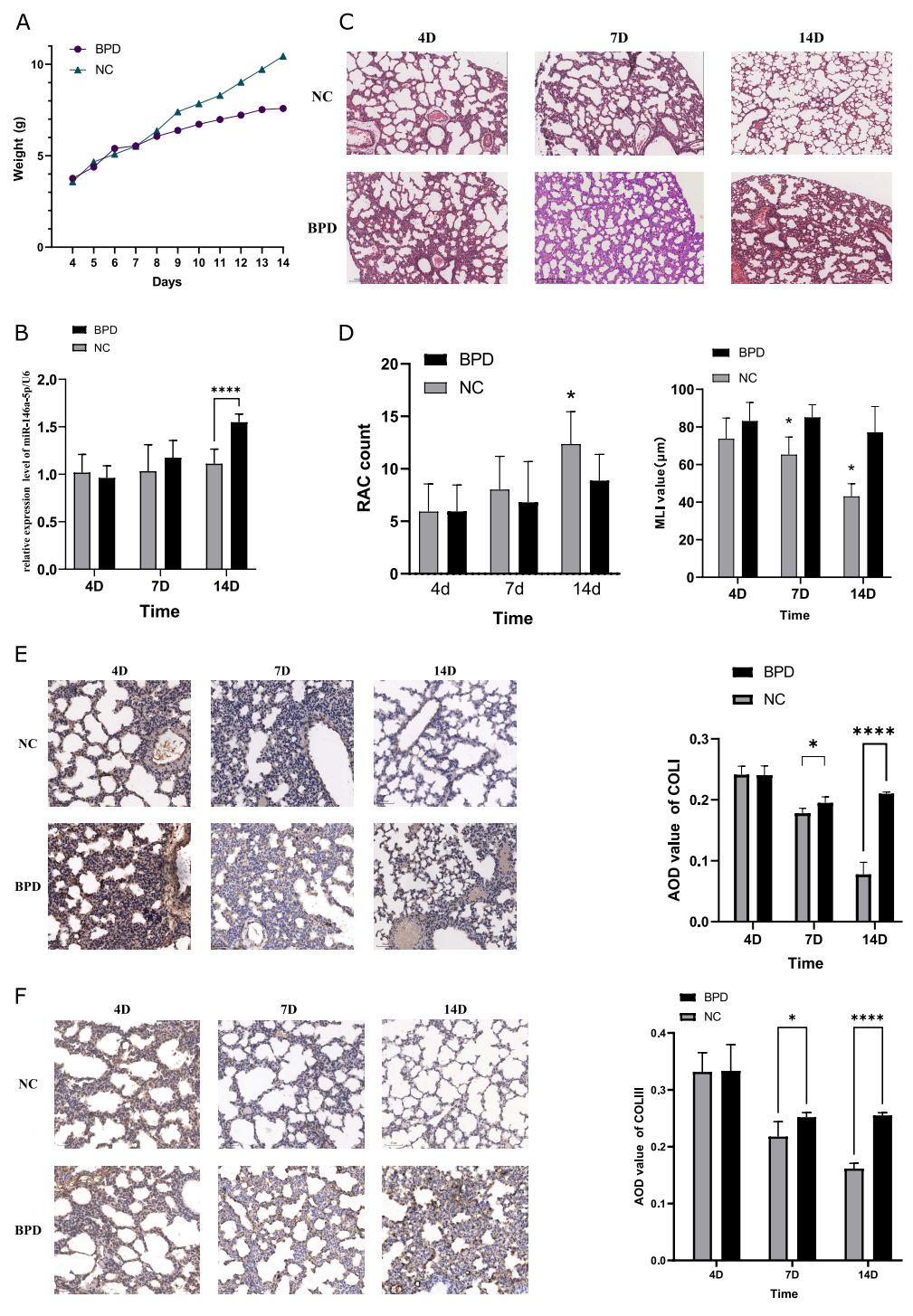


Fig. 3 Increased expression of miR-146a-5p and elevated levels of fibrosis factors were observed in the underdeveloped lung tissues of neonatal mice with BPD over a span of time. (A) The weight changes between the NC and BPD groups in the 14 days observation. The BPD group's weight gained slower than the NC group. (B) The levels of miR-146a-5p expression in lung tissues of BPD group as determined by RT-qPCR and normalized to U6. (C) H&E staining of pulmonary microvascular (\times 100). (D) The RAC and MLI counts for each group of mice. (E) and (F) Immunohistochemistry half-quantification of the fibrosis factor of COL I and observed (\times 200) and COL III and observed (\times 200), respectively. Data are summarized as mean \pm standard deviation. * p < 0.05 vs. NC group. Data comparisons between multiple groups were performed using two-way ANOVA and Bonferroni's for post hoc test. n = 5 for mice in each group. RAC = radial alveolar counts; MLI = mean linear intercept; AOD = average optical density.

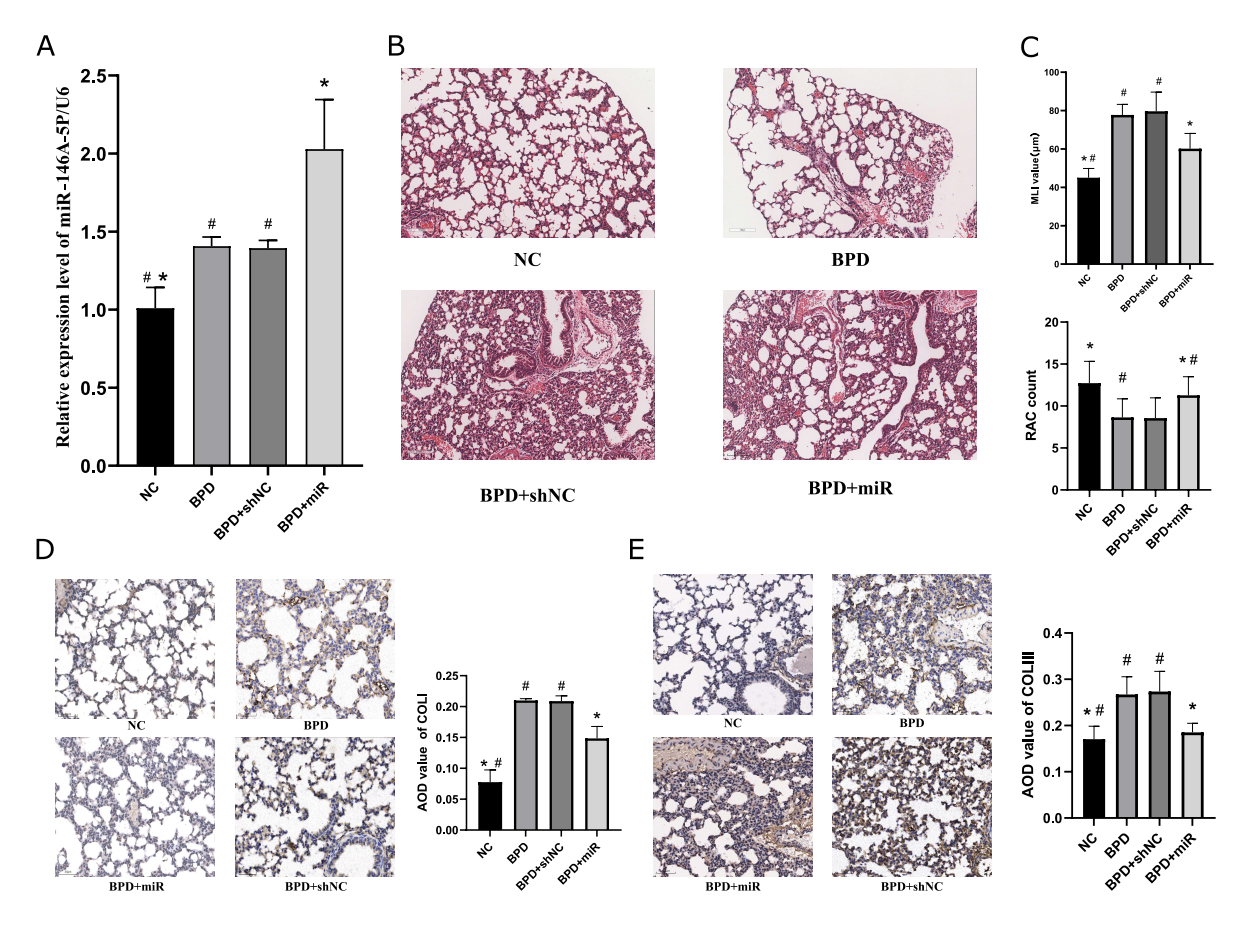


Fig. 4 Overexpressed level of miR-146a-5p in the lung tissue of neonatal mice with BPD could restore alveolarization. (A) The levels of miR-146a-5p expression in lung tissues after the inhaled of the miR-146a-5p lentivirus vectors as determined by RT-qPCR and normalized to U6. (B) H&E staining of pulmonary microvascular (×100). (C) The RAC and MLI counts for each group of mice. (D) and (E) Immunohistochemistry half-quantification of the fibrosis factor of COL I and observed (×200), and COL III and observed (×200), respectively. Data are summarized as mean \pm standard deviation. * p < 0.05 vs. BPD group. * p < 0.05 vs. BPD+miR group. Data comparisons between multiple groups were performed using one-way ANOVA and Tukey's for post hoc test. p = 0.05 in each group. RAC = radial alveolar counts; MLI = mean linear intercept; AOD = average optical density.

TGF-β pathway, thereby restraining mice bronchopulmonary fibrosis and alveoli simplification.

DISCUSSION

Bronchopulmonary dysplasia is a common chronic lung disease in premature infants, with an unclear pathogenesis and limited treatment options. Perinatal risk factors for BPD include chorioamnionitis [20], maternal smoking, gestational hypertension [21], and intrauterine growth restriction. Postnatal risk factors include mechanical ventilation, high oxygen concentration, infection, pulmonary inflammation, patent ductus arteriosus (PDA), and malnutrition [22, 23].

Research by Koussa et al [24] and Siddaiah et al [25] has shown that the dysregulation of multiple microRNAs is associated with the pathogenesis of BPD. For example, miR-378b, miR-184, miR-3667-5p, miR-3976, miR-4646-5p, and miR-7846-3p are up-regulated in the lung tissue of BPD patients,

while the expression levels of several other microR-NAs are significantly decreased. miR-146a, a member of the microRNA family, is involved in the pathophysiological processes of various respiratory diseases, such as severe lower respiratory tract bronchiolitis and asthma [26], novel coronavirus pneumonia [27], and hypoxic lung injury [28]. miR-146a-5p plays a significant role in fibrosis processes in organs such as the liver and heart [29–31]. Our research indicates that miR-146a-5p is up-regulated in neonatal mice with oxygen-induced BPD, and its over-expression can reverse lung inflammation and fibrosis. Therefore, miR-146a-5p may play a crucial role in the pathogenesis of BPD and has the potential to be used as a biomarker.

Combining bioinformatics analysis and dual-luciferase assay results, we speculate that miR-146a-5p may exert a protective effect in BPD by mediating the TGF- β 1/SMAD4 pathway. TGF- β 1/SMAD4 is closely associated with the occurrence and development of

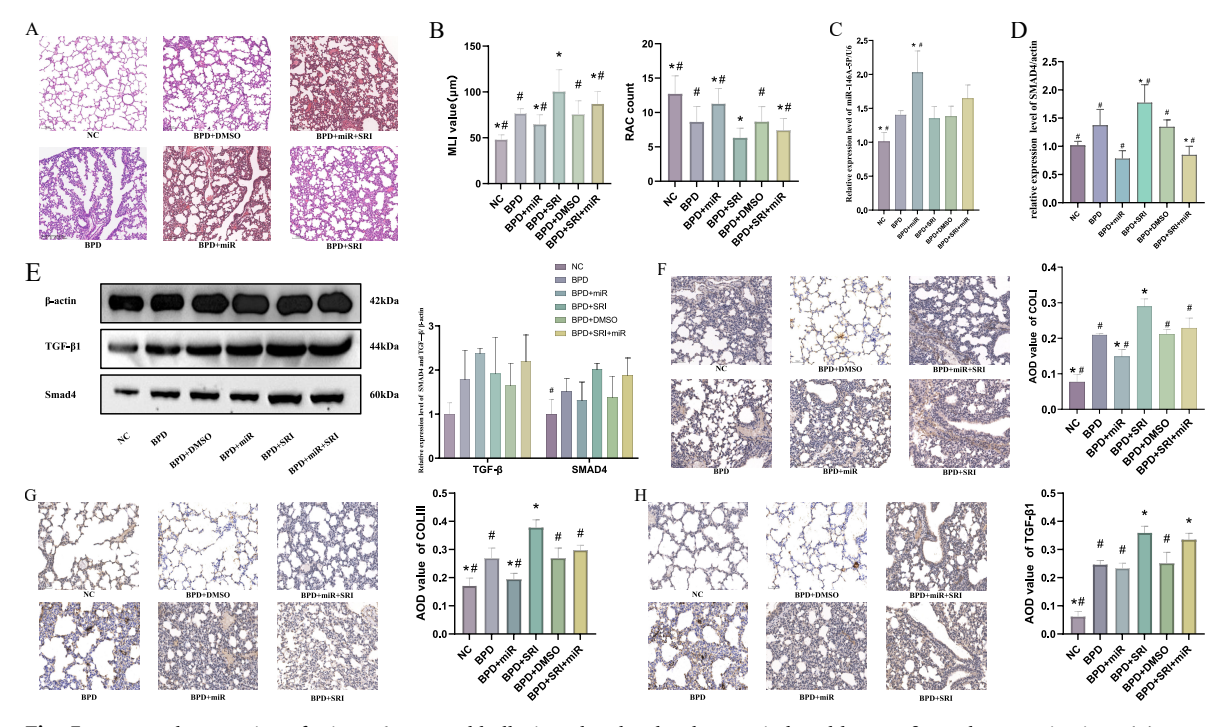


Fig. 5 Increased expression of miR-146a-5p could alleviate the alveolar damage induced by TGF-β1 pathway activation. (A) H&E staining of pulmonary microvascular (×100). (B) H&E staining showing the number of alveoli, and alveolar diameter. (C) The levels of miR-146a-5p expression in lung tissues of BPD group after treated with SRI-011381 as determined by RT-qPCR and normalized to U6. (D) The levels of SMAD4 mRNA expression in lung tissues after the as determined by RT-qPCR and normalized to actin. (E) Western blot analysis of the activation of the TGF-β pathway in BPD neonatal mice normalized to β-actin (n = 3). (F), (G), and (H) Immunohistochemistry half-quantification of the fibrosis factor of COL I, COL III, and TGF-β1, respectively. Data are summarized as mean ± standard deviation. * p < 0.05 vs. BPD group. *p < 0.05 vs. BPD+SRI group. Data comparisons between multiple groups were performed using one-way ANOVA and Tukey's for post hoc test. n = 5 for mice in each group. RAC = radial alveolar counts; MLI = mean linear intercept; AOD = average optical density.

organ fibrosis [32, 34]. In our study, when TGF-β1 and SMAD4 were stimulated, lung inflammation and fibrosis in mice worsened, with increased inflammation exudation, thickening of alveolar septa, more pronounced alveolar cavity enlargement, and increased fibrosis, along with up-regulation of downstream factors COL I and COL III in the lungs of BPD mice. This is consistent with other studies [35]. Furthermore, the over-expression of miR-146a-5p can down-regulate SMAD4 levels, affecting the expression of downstream COL I and COL III, and improving lung conditions in mice (Fig. 6). In addition, Curcio et al [36] reported that miR-146a-5p can exert anti-inflammatory effects by acting on NLRP3 or NLRP4 inflammasomes in patients with COVID-19-related acute respiratory distress syndrome. Other studies have shown that miR-146a-5p can target SMAD4 to regulate osteoblast apoptosis [37]. In this study, the assessment of other molecular levels in the TGF-β pathway, such as the levels of phosphorylated SMAD2/SMAD3 that form complexes with SMAD4, is still lacking. Given the multitude of target genes associated with miRNAs, it is plausible that miR-146a-5p could also mitigate lung injury in BPD via additional pathways. This possibility deserves further exploration and validation through preclinical and clinical evidence.

Additionally, due to the application of prenatal corticosteroids, pulmonary surfactant, and lung protective ventilation in premature infants, the etiology of BPD has shifted from lung injury caused by improper respiratory support and oxygen use to pulmonary alveolar simplification and abnormal pulmonary vascular development due to lung developmental disorders in premature infants. The new type of BPD is characterized pathologically by larger, simplified cystic alveoli, irregular pulmonary vasculature, and mild pulmonary fibrosis. The hyperoxia-induced BPD model used in this study is histologically more similar to pulmonary fibrosis and old BPD, with limited simulation of the new type of BPD and insufficient assessment of the effects of hyperoxia on other organs besides the lungs [38, 39]. At the same time, when assessing lung injury in BPD model mice, measurements of MLI and RAC may be biased, and the use of lung function tests or computed tomography and magnetic resonance imaging may also help to identify and distinguish

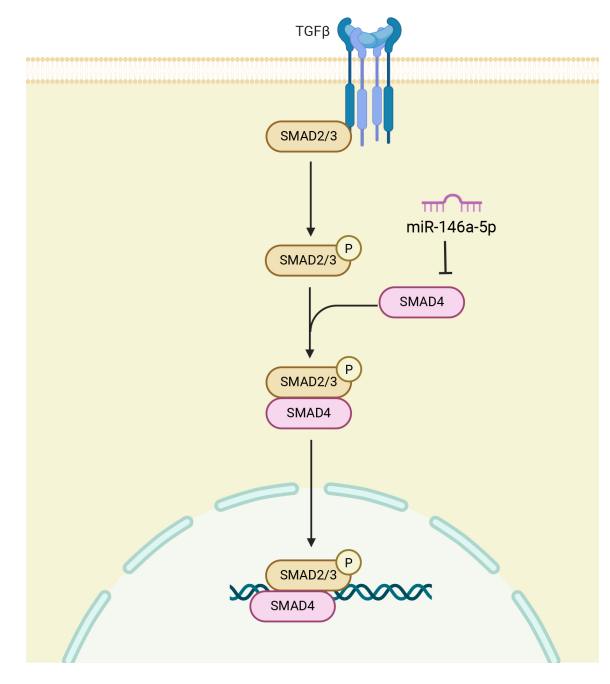


Fig. 6 miR-146a-5p targets SMAD4 to regulate signals in TGF- β pathway.

pulmonary abnormalities caused by hyperoxia-induced lung injury [38, 40]. Further clinical translation still requires a substantial amount of research.

Based on previous studies and our preliminary experimental exploration, we believe that miR-146a-5p can regulate the TGF- β 1 pathway by targeting SMAD4 to reduce the expression of COL I and COL III, thereby improving lung inflammation and fibrosis in BPD mice.

Appendix A. Supplementary data

Supplementary data associated with this article can be found at https://dx.doi.org/10.2306/scienceasia1513-1874.2025.

Acknowledgements: This study is supported by the Natural Science Foundation of Fujian Province, 2021J0112.

REFERENCES

- Northway WJ, Rosan R, Porter DY (1967) Pulmonary disease following respirator therapy of hyaline-membrane disease Bronchopulmonary dysplasia. *Engl J Med* 276, 357–368.
- Schmidt AR, Ramamoorthy C (2022) Bronchopulmonary dysplasia. Paediatr Anaesth 32, 174–180.
- Bancalari E, Jain D (2019) Bronchopulmonary dysplasia: 50 years after the original description. *Neonatology* 115, 384–391.
- Deng X, Bao Z, Yang X, Mei Y, Zhou Q, Chen A, Yu R, Zhang Y (2023) Molecular mechanisms of cell death in bronchopulmonary dysplasia. *Apoptosis* 28, 39–54.
- Perrone S, Manti S, Buttarelli L, Petrolini C, Boscarino GA-O, Filonzi L, Gitto E, Esposito SMR, et al (2023) Vascular endothelial growth factor as molecular target

- for bronchopulmonary dysplasia prevention in very low birth weight infants. *Int J Mol Sci* **24**, 2729.
- Wang H, Yan D, Wu Z, Geng H, Zhu X, Zhu X (2023) Predictive values of clinical data, molecular biomarkers, and echocardiographic measurements in preterm infants with bronchopulmonary dysplasia. *Front Pediatr* 10, 1070858.
- Akat A, Yilmaz Semerci S, Ugurel OM, Erdemir A, Danhaive O, Cetinkaya M, Turgut-Balik D (2022) Bronchopulmonary dysplasia and wnt pathwayassociated single nucleotide polymorphisms. *Pediatr Res* 92, 888–898.
- 8. Wang M, Xie H, Mi S, Chen J (2007) Recent patents on the identification and clinical application of microRNAs and target genes. *Recent Pat DNA Gene Seq* 1, 116–124.
- Schickel R, Boyerinas B, Park S-M, Peter ME (2008) MicroRNAs: key players in the immune system, differentiation, tumorigenesis and cell death. *Oncogene* 27, 5959–5974
- 10. Sano M, Akagi D, Naito M, Hoshina K, Miyata K, Kataoka K, Ishihara S (2022) Systemic single administration of anti-inflammatory microRNA 146a-5p loaded in polymeric nanomedicines with active targetability attenuates neointimal hyperplasia by controlling inflammation in injured arteries in a rat model. FASEB J 36, e22486.
- 11. Sun W, Ma J, Zhao H, Xiao C, Zhong H, Ling H, Xie Z, Tian Q, et al (2020) Resolvin D1 suppresses pannus formation via decreasing connective tissue growth factor caused by upregulation of miRNA-146a-5p in rheumatoid arthritis. *Arthritis Res Ther* **22**, 61.
- Chen Q, Lin J, Deng Z, Qian W (2022) Exosomes derived from human umbilical cord mesenchymal stem cells protect against papain-induced emphysema by preventing apoptosis through activating VEGF-VEGFR2-mediated AKT and MEK/ERK pathways in rats. Regen Ther 21, 216–224.
- 13. Dong L, Wang Y, Zheng T, Pu Y, Ma Y, Qi X, Zhang W, Xue F, et al (2021) Hypoxic hUCMSC-derived extracellular vesicles attenuate allergic airway inflammation and airway remodeling in chronic asthma mice. Stem Cell Res Ther 12. 4.
- 14. Wang Q, Hu Q, Ying Y, Lu C, Li W, Huang C, Xu W, Li Q, et al (2021) Using next-generation sequencing to identify novel exosomal miRNAs as biomarkers for significant hepatic fibrosis. *Discov Med* **31**, 147–159.
- Cai P, Mu Y, Olveda RM, Ross AG, Olveda DU, Mc-Manus DP (2018) Circulating miRNAs as footprints for liver fibrosis grading in schistosomiasis. *EBioMedicine* 37, 334–343.
- 16. Gronau L, Duecker RP, Jerkic SP, Eickmeier O, Trischler J, Chiocchetti AG, Blumchen K, Zielen S, et al (2024) Dual role of microRNA-146a in experimental inflammation in human pulmonary epithelial and immune cells and expression in inflammatory lung diseases. *Int J Mol Sci* 25, 7686.
- 17. Zhang M, Ma T, Hu B, Xiang W (2022) FOXP1 promotes osteoblast differentiation via regulation of TGF-β/ALK-5 pathway. *ScienceAsia* **48**, 423–428.
- Hu HH, Chen DQ, Wang YN, Feng YL, Cao G, Vaziri ND, Zhao Y-Y (2018) New insights into TGF-β/Smad signaling in tissue fibrosis. *Chem Biol Interact* 292, 76–83.
- 19. Li YJ, Azuma A, Usuki J, Abe S, Matsuda K, Sunazuka T, Shimizu T, Hirata Y, et al (2006) EM703 improves

- bleomycin-induced pulmonary fibrosis in mice by the inhibition of TGF-beta signaling in lung fibroblasts. *Respir Res* **7**, 16.
- Jain VG, Parikh NA, Rysavy MA, Shukla VV, Trotta M, Jobe A, Carlo WA, Ambalavanan N (2024) Histological chorioamnionitis increases the risk of bronchopulmonary dysplasia. Am J Respir Crit Care Med 209, 1272–1275.
- 21. Morrow LA, Wagner BD, Ingram DA, Poindexter BB, Schibler K, Cotten CM, Dagle J, Sontag MK, et al (2017) Antenatal determinants of bronchopulmonary dysplasia and late respiratory disease in preterm infants. *Am J Respir Crit Care Med* 196, 364–374.
- Nawaytou H, Hills NK, Clyman RI (2023) Patent ductus arteriosus and the risk of bronchopulmonary dysplasiaassociated pulmonary hypertension. *Pediatr Res* 94, 547–554.
- 23. Jiang H, Lv Y, Hou W, Xu X, Zhu L, Zhang H, Shu G (2022) Association between neonatal malnutrition and bronchopulmonary dysplasia in very low-birth-weight infants: A propensity score-matched analysis. *Nutr Clin Pract* 37, 1429–1437.
- Koussa S, Dombkowski A, Cukovic D, Poulik J, Sood BG (2023) MicroRNA dysregulation in the heart and lung of infants with bronchopulmonary dysplasia. *Pediatr Pul-monol* 58, 1982–1992.
- Siddaiah R, Oji-Mmuo CN, Montes DT, Fuentes N, Spear D, Donnelly A, Silveyra P (2021) MicroRNA signatures associated with bronchopulmonary dysplasia severity in tracheal aspirates of preterm infants. *Biomedicines* 9, 257
- 26. Rodrigo-Muñoz JM, Gil-Martínez M, Lorente-Sorolla C, Sastre B, García-García ML, Calvo C, Casas I, del Pozo V (2022) Reduced miR-146a-5p is a biomarker of infant respiratory diseases contributing to immune dysregulation in small airway epithelial cells. *Cells* 11, 2746.
- 27. Meidert AS, Hermann S, Brandes F, Kirchner B, Buschmann D, Billaud JN, Klein M, Lindemann A, et al (2021) Extracellular vesicle associated miRNAs regulate signaling pathways involved in COVID-19 pneumonia and the progression to severe acute respiratory corona virus-2 syndrome. Front Immunol 12, 784028.
- 28. Lin G, Huang J, Chen Q, Chen L, Feng D, Zhang S, Huang X, Huang Y, et al (2019) miR-146a-5p mediates intermittent hypoxia-induced injury in H9c2 cells by

- targeting XIAP. Oxid Med Cell Longev 2019, 6581217.
- Yuan BY, Zhuang Y, Wu ZF, Zhao XM, Zhang L, Chen GW, Zeng ZC (2023) miR-146a-5p alleviates radiationinduced liver fibrosis by regulating PTPRA-SRC signaling in mice. *Radiat Res* 200, 531–537.
- 30. Zhang H, Wen H, Huang Y (2022) MicroRNA-146a attenuates isoproterenol-induced cardiac fibrosis by inhibiting FGF2. *Exp Ther Med* **24**, 506.
- 31. Tabios IKB, Sato MO, Tantengco OAG, Fornillos RJC, Kirinoki M, Sato M, Rojo RD, Fontanilla IKC, et al (2022) Circulating microRNAs as biomarkers of hepatic fibrosis in schistosomiasis japonica patients in the Philippines. *Diagnostics* **12**, 1902.
- 32. Bataller R, Brenner DA (2005) Liver fibrosis. *J Clin Invest* 115, 209–218.
- 33. Iredale JP (2007) Models of liver fibrosis: exploring the dynamic nature of inflammation and repair in a solid organ. *J Clin Invest* 117, 539–548.
- 34. Clouthier DE, Comerford SA, Hammer RE (1997) Hepatic fibrosis, glomerulosclerosis, and a lipodystrophy-like syndrome in PEPCK-TGF-beta1 transgenic mice. *J Clin Invest* **100**, 2697–2713.
- 35. Shen YQ, Bao ZD, Pan JJ, Mao XN, Cheng R, Zhou XG, Zhou X-Y, Yang Y (2020) MicroRNA-431 inhibits the expression of surfactant proteins through the BMP4/activin/TGF-β signaling pathway by targeting SMAD4. *Int J Mol Med* **45**, 1571–1582.
- 36. Curcio R, Poli G, Fabi C, Sugoni C, Pasticci MB, Ferranti R, Rossi M, Folletti I, et al (2023) Exosomal miR-17-5p, miR-146a-3p, and miR-223-3p correlate with radiologic sequelae in survivors of COVID-19-related acute respiratory distress syndrome. *Int J Mol Sci* 24, 13037.
- 37. Liu X, Zhang K, Wang L, Geng B, Liu Z, Yi Q, Xia Y (2022) Fluid shear stress-induced down-regulation of miR-146a-5p inhibits osteoblast apoptosis via targeting SMAD4. *Physiol Res* **71**, 835–848.
- Giusto K, Wanczyk H, Jensen T, Finck C (2021) Hyperoxia-induced bronchopulmonary dysplasia: better models for better therapies. *Dis Model Mech* 14, dmm047753.
- 39. Ozdemir SH, Ovali HF (2024) Association of acute kidney injury with bronchopulmonary dysplasia in preterm infants. *Medeniyet Med J* **39**, 152–160.
- 40. Berger J, Bhandari V (2014) Animal models of bronchopulmonary dysplasia. The term mouse models. *Am J Physiol Lung Cell Mol Physiol* **307**, L936–947.

Appendix A. Supplementary data

 Table S1
 RT-qPCR primer sequences.

Gene	Sequence
U6	F:5'-CTCGCTTCGGCAGCACA-3'
U6	R:5'-AACGCTTCACGAATTTGCGT-3'
mmu-miR-146a-5p	F:5'-CCGCGCTGAGAACTGAATTCCA-3'
mmu-miR-146a-5p	R:5'-AGTGCAGGGTCCGAGGTATT-3'
β-actin	F:5'-TGACGTGGACATCCGCAAAG-3'
β-actin	R:5'-CTGGAAGGTGGACAGCGAGG-3'
SMAD4	F:5'-AGGTGGCCTGATCTACACAAG-3'
SMAD4	R:5'-ACCCGCTCATAGTGATATGGATT-3'